

# CO Generation from CO<sub>2</sub> Using an Atmospheric Microwave Plasma Process

Marc Bresser\*, Katharina Wieggers, Andreas Schulz, Matthias Walker  
and Günter E. M. Tovar

DOI: 10.1002/cite.202400157

 This is an open access article under the terms of the [Creative Commons Attribution](#) License, which permits use, distribution and reproduction in any medium, provided the original work is properly cited.

With rising CO<sub>2</sub> levels and climate change, finding alternatives to fossil fuels is essential. One attractive option is converting CO<sub>2</sub> into CO and O<sub>2</sub> via an atmospheric microwave plasma process. This study evaluates conversion and energy efficiency by increasing microwave power and CO<sub>2</sub> flow. Power and CO<sub>2</sub> flow were varied, with conversion measured using Fourier transform-infrared spectroscopy, mass spectrometry, and gas analysis. A maximum conversion of 21.1 % was achieved at a specific energy input of 1.1 eV molecule<sup>-1</sup>, highlighting the potential of this approach for efficient CO<sub>2</sub> utilization.

**Keywords:** Atmospheric microwave plasma torch, CO generation, CO<sub>2</sub> plasma, Plasma chemistry, Plasma technology

*Received:* November 29, 2024; *revised:* January 29, 2025; *accepted:* February 06, 2025

## 1 Introduction

CO<sub>2</sub> represents the naturally occurring carbon building block of the carbon cycle, which is completely oxidized and therefore in its lowest energetic state. In the natural cycle, photosynthesis activates this building block and converts it into chemically reduced carbon building blocks. However, since the beginning of industrialization, natural photosynthesis can no longer keep up with the CO<sub>2</sub> emissions caused by humans, which has led to an increase in the CO<sub>2</sub> concentration in the atmosphere.

CO<sub>2</sub> is the biggest factor influencing the rise in temperature [1]. Aforementioned rose from 300 ppm in 1900 to 410 ppm in 2019 [2], which in turn led to an increase in the global surface temperature by 1.1 °C in between 2010 and 2019 compared to pre-industrial conditions due to the greenhouse effect. The annual global anthropogenic greenhouse gas (GHG) emissions were estimated for 59 ± 6.6 GtCO<sub>2</sub>-eq in 2019. The energy sector produced around 34 % of GHGs in 2019 and the industrial sector 24 % [2]. These high values are due to the intensive use of fossil fuels for energy and materials, driving CO<sub>2</sub> emissions. Due to global warming, the United Nations passed the Paris Agreement [3] to reduce climate change. The global surface temperature limit was set at 2 °C (preferably below 1.5 °C) above the pre-industrial levels. To achieve this, the GHG concentration in the atmosphere has to be lowered drastically.


In today's economy, industries are heavily dependent on fossil fuels and thus directly contribute to the production of GHGs. One way to achieve a renewable future is by using renewable energy and exploring new synthesis routes to


enable a sustainable carbon economy. An attractive starting point is to take CO<sub>2</sub> as a reactant for carbon-based chemicals and close the carbon cycle [4]. Carbon monoxide (CO), as a product of CO<sub>2</sub>, can be used by adding green hydrogen to form a fully sustainable syngas [5]. This provides a renewable feedstock for methanol, ethanol, dimethyl ether, fuels, and other carbon-based chemicals [6].

The state-of-the-art process to produce syngas is by steam reforming of natural gas [7] or by partial oxidation of methane [6]. New approaches to produce syngas have to be discovered. Green hydrogen can be produced sustainably through electrolysis of water, using renewable energy [8, 9]. Additionally, carbon monoxide (CO) can be obtained by the reduction of CO<sub>2</sub>. A variety of processes have been proven to achieve this, e.g., electrochemically through electrolysis, thermal splitting, biochemically, photochemically, solar thermochemically, catalytically or with a plasma process [10–12]. A plasma splits CO<sub>2</sub> into CO and O<sub>2</sub> via the

<sup>1</sup>Marc Bresser  <https://orcid.org/0009-0002-3773-4764>


([marc.bresser@igvp.uni-stuttgart.de](mailto:marc.bresser@igvp.uni-stuttgart.de)), <sup>1</sup>Katharina Wieggers

 <https://orcid.org/0009-0002-0307-9300>, <sup>1</sup>Dr. Andreas Schulz

 <https://orcid.org/0009-0009-7611-4702>, <sup>1</sup>Dr. Matthias Walker

 <https://orcid.org/0000-0001-9251-4356>,

<sup>1,2</sup>Prof. Dr. Günter E. M. Tovar

 <https://orcid.org/0000-0002-2437-3405>

<sup>1</sup>University of Stuttgart, Institute of Interfacial Process Engineering and Plasma Technology (IGVP), Pfaffenwaldring 31, 70569 Stuttgart, Germany.

<sup>2</sup>Fraunhofer Institute for Interfacial Process Engineering and Biotechnology IGB, Fraunhofer-Network Nanotechnology, Nobelstr. 12, 70569 Stuttgart, Germany.

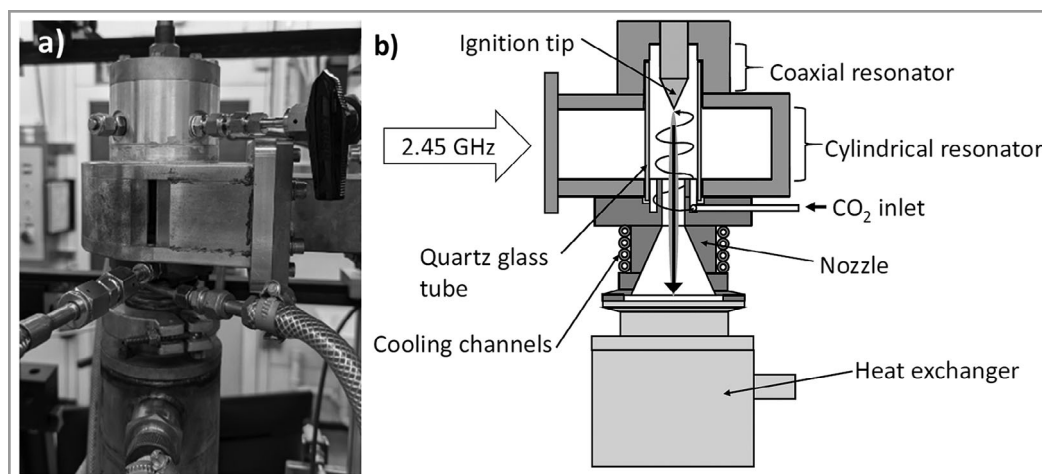


**Figure 1.** Photo of the plasma torch (a) and schematic drawing of the atmospheric pressure microwave plasma torch with a 13 mm nozzle in reverse vortex configuration (b).

following reaction formula:



The quenching of the reaction after the plasma is important to prevent the back reaction to  $\text{CO}_2$  at lower temperatures and to achieve high conversion efficiencies [13]. The  $\text{CO}_2$  conversion  $\chi$  is calculated with the measured  $\text{CO}_2$  concentration in vol.-% in the product according to:

$$\chi = \frac{1 - \text{vol \% CO}_2}{1 + 0.5 \text{ vol \% CO}_2} \quad (2)$$

The amount of produced CO product can be calculated with Eq. (3):

$$F(\text{CO})[\text{L} \cdot \text{min}^{-1}] = \chi * F_{\text{in}}(\text{CO}_2)[\text{L} \cdot \text{min}^{-1}] \quad (3)$$

The specific energy input (SEI) defines the energy per volume unit of reactant gas and is needed to calculate energy efficiency (EE). It is calculated with the following formula:

$$\text{SEI} [\text{kJ} \cdot \text{L}^{-1}] = \frac{P [\text{kW}]}{F_{\text{in}}(\text{CO}_2) [\text{L} \cdot \text{min}^{-1}]} * 60 [\text{s} \cdot \text{min}^{-1}] \quad (4)$$

The EE is determined by:

$$\eta [\%] = \frac{\Delta H_{\text{R}} [\text{kJ} \cdot \text{mol}^{-1}] * \chi (\text{CO}_2) [\%]}{\text{SEI} [\text{kJ} \cdot \text{L}^{-1}] * 24.1 [\text{L} \cdot \text{mol}^{-1}]} \quad (5)$$

In Eq. (5)  $\Delta H_{\text{R}}$  (2.9 eV molecule<sup>-1</sup>) is the reaction enthalpy for  $\text{CO}_2$  splitting at 298 K, and 24.1 L mol<sup>-1</sup> is the molar volume for ideal gases.

In this work, a microwave plasma torch at atmospheric pressure is used to split  $\text{CO}_2$ . The torch was designed and developed in our institute and is operating at a frequency of 2.45 GHz [14–18]. The advantage of the used setup is that it is self-igniting, requires a short time to turn on, and

is flexible in the electrical power used. The fluctuations of renewable energies can be used with this plasma process. Another benefit compared to other technologies is that no electrodes are employed and no rare earth materials are required. This plasma torch resonator was applied for  $\text{CO}_2$  conversion experiments at microwave powers up to 1.6 kW and  $\text{CO}_2$  flows up to 12 slm [19].

The resonator structure was also investigated at 60–1000 mbar, varied nozzles, with an additional membrane reactor or different quenching configurations [13, 20–26]. A similar reactor structure was set up for 915 MHz [27, 28] and was tested at 200 mbar for  $\text{CO}_2$  conversion [29]. The advantages of using 915 MHz are that the reactor is bigger, so higher microwave powers and gas flow rates are possible. Additionally, the magnetron efficiency is higher compared to 2.45 GHz. For industrial applications, 915 MHz is more appealing and an innovative way to scale up the plasma process. In this work, different diagnostics are tested and compared on two different plasma systems. The influence of  $\text{CO}_2$  flow rate and microwave power on produced CO flow and energy efficiency was measured. The first step for upscaling was taken with microwave powers up to 5.7 kW and  $\text{CO}_2$  gas flows up to 74 slm.

## 2 Experimental Setup

### 2.1 Microwave Plasma Torch, Nozzle, and Heat Exchanger

The microwave plasma torch shown in Fig. 1 consists of a coaxial and a cylindrical resonator. The coaxial resonator has a narrow bandwidth, while the cylindrical resonator has a broad bandwidth. A quartz glass tube with an inner diameter of 26 mm and an outer diameter of 30 mm forms the reactor volume. To a resonance to occur, the ignition tip has

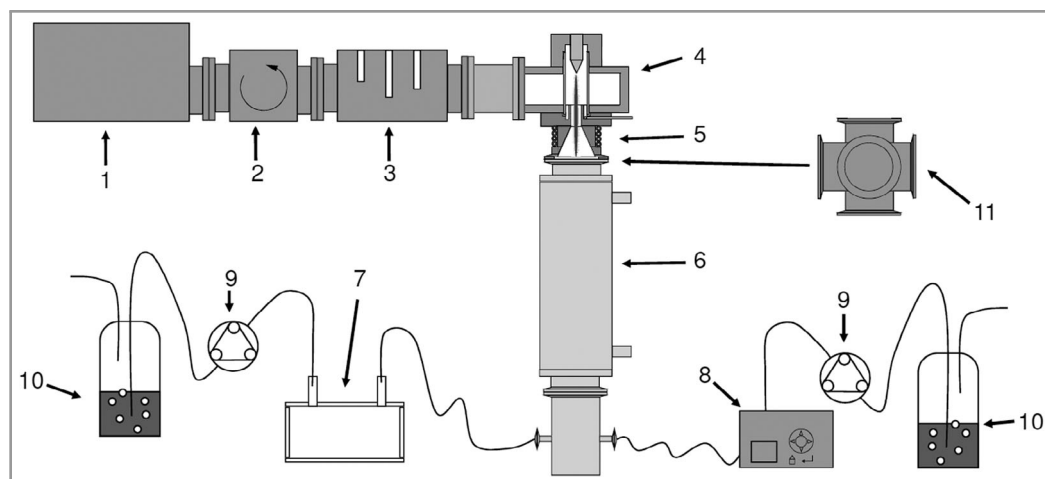


**Figure 2.** Schematic representation of atmospheric pressure microwave plasma torch and product gas diagnostics in the cooled down gas stream. The system consists of a magnetron (1), circulator (2), 3-stub tuner (3), plasma torch (4), nozzle (5), heat exchanger (6), FT-IR gas cell (7), gas analyzer (8), peristaltic pump (9), and a glass container filled with water (10) and the optional membrane reactor (11).

a length of  $\lambda/4$ . The wavelength of a microwave at a frequency of 2.45 GHz is 122.5 mm. The vertical position of the ignition tip can be adjusted with the network analyzer (Pico vector Network Analyzer PicoVNA 108 300 kHz–8.5 GHz Quad RX) and the connected analysis software (Pico VNA2 Control v2.11), so that resonance can occur. The microwaves couple into the coaxial resonator and generate a maximal electric field at the tip of the inner conductor of the coaxial resonator. This leads to the so-called self-ignition of the plasma. The plasma moves to the cylindrical resonator within milliseconds [28]. At that position, the plasma absorbs nearly all the incoming microwave power and is maintained in the cylindrical resonator.

The  $\text{CO}_2$  gas is introduced into the plasma torch through up to four symmetrically arranged tangential gas inlets in the quenching nozzle. In this work, only up to two inlets were used. The gas inlets have an inner diameter of 4 mm. At gas flow rates higher than 37 slm an additional second gas inlet was used in a  $180^\circ$  angle and the gas flows were equally distributed. For the plasma process,  $\text{CO}_2$  of 99.995 % purity distributed by the company Widman Gase GmbH was used. The gas inlet creates an upwards vortex flow inside the quartz glass tube. The vortex stabilizes the plasma in the middle of the tube and protects the glass against thermal damage. At the end of the cylindrical resonator the vortex turns at the ignition tip and goes through the plasma zone. This configuration is called reverse vortex configuration. An advantage of this configuration is a stable plasma process that allows most of the introduced gas to pass through the reaction zone. Behind the reaction zone a nozzle with 13 mm in diameter was mounted on the exit of the resonator. The nozzle quenches the plasma, preventing the back reaction of CO and O to  $\text{CO}_2$ . The nozzle has an opening angle of

$60^\circ$  on the side of the heat exchanger. The heat exchanger is operated at atmospheric pressure and consists of copper pipes that are cooled with water.

The used scaled-up plasma process is compared to the plasma system presented by Wiegers et al. [25]. The two setups are equipped with the same plasma torch and nozzle. The differences between the plants are the magnetron, the generator, and the analytics for the product gas. Wiegers et al. [19] used a magnetron with a maximum microwave power of 2 kW. The microwave plasma plant used in this work with a microwave power up to nominal 6 kW is schematically illustrated in Fig. 2.

This plant consisted of a magnetron of the company MUEGGE (MH6000S-250BF) and a generator from MUEGGE (MX6000D-15IKL). A circulator with a water-load and a 3-stub tuner were connected to the magnetron. The circulator protects the magnetron from reflected power while the automated 3-stub tuner matches the impedance of the incoming and reflected wave. Through the adjustment of the stubs the reflected power is smaller than the detection limit for the reflected power and therefore almost all of the power is absorbed by the plasma. The software HomTool 5.0.0.4, by S-TEAM of the 3-stub tuner measures the incoming and reflected power, so that the actual power going into the plasma can be quantified. Behind the torch and the nozzle, a heat exchanger was installed. Only for the experiments to compare with Wiegers et al. [25] a membrane reactor was installed between the nozzle and the heat exchanger. In this case, no membranes were used and the reactor only creates a distance between the nozzle and the heat exchanger. The quenching of the hot effluent plasma was ensured with the nozzle and a heat exchanger. The cooled-down product gas behind the heat exchanger was measured in a bypass

configuration with a Fourier transform-infrared (FT-IR) spectrometer and a gas analyzer. Post-diagnostically a peristaltic pump with a constant flow rate and a bubbler was installed.

## 2.2 Product Gas Diagnostics

The different diagnostics were all installed in a bypass behind the heat exchanger. In the setup with the 2 kW magnetron a mass spectrometer (MS) from Pfeiffer (Prisma Plus QMG 220 M2) and an FT-IR absorption spectrometer from Bruker (Vector22) were installed. The gases at the plant with the 6 kW magnetron were analyzed with an FT-IR spectrometer from Bruker (Invenio R) at atmospheric pressure and a continuous gas analyzer from Emerson (Rosemount X-Stream Enhanced XEGP). Behind the two diagnostics, a peristaltic pump for a constant gas flow and a bubbler to check the functionality of the pump were installed. The background of the FT-IR spectrometer was made with  $N_2$ . The calibration and measurement procedure of the MS and the FT-IR spectrometer are described in detail in Wiegers et al. [19].

In case of the FT-IR spectrometer the bands were analyzed with the software OPUS 7.8. The  $CO_2$  band of the combination band at  $4983\text{ cm}^{-1}$  was used for the determination of the  $CO_2$  concentration and for CO the signal at  $4250\text{ cm}^{-1}$  was selected [30–32]. The gas analyzer was equipped with four different channels for the gases  $CO_2$ , CO,  $O_2$ , and  $H_2$ . CO and  $CO_2$  were quantified with an IR detector,  $O_2$  with a paramagnetic sensor, and  $H_2$  with a thermal conductivity detector. The gas analyzer calibration was carried out by introducing the gases into the resonator of the system, just as in the running plasma process.  $CO_2$  and  $O_2$  were calibrated in a range of 0 to 100 %. CO was calibrated from 0 to 50 % with an admixture of  $CO_2$ . The calibration was carried out after 20 min at an equilibrium. Each datapoint was measured three different times over a time span of each 15 min and the mean value was calculated. The maximum error for a datapoint per gas was found at 1.5 %. For calibration, the following gases were used:  $CO_2$  of 99.995 % purity (Widman Gase GmbH), CO 99.9 % (KRAISS & FRIZ Gase und Technik GmbH & Co. KG), and  $O_2$  99.995 % (KRAISS & FRIZ Gase und Technik). As background and purging gas, nitrogen of 99.999 % purity (KRAISS & FRIZ Gase und Technik) was utilized.

## 3 Results and Discussion

The previous publication of Wiegers et al. [25] showed a very good comparability of the two diagnostics MS and FT-IR spectrometry [19]. In addition to the setup as displayed in Fig. 2, the membrane reactor was mounted between the nozzle and the heat exchanger like the setup from Wiegers et al. [25] to compare the plasma torches and the different diagnostics. To verify the outcomes produced by the 6 kW

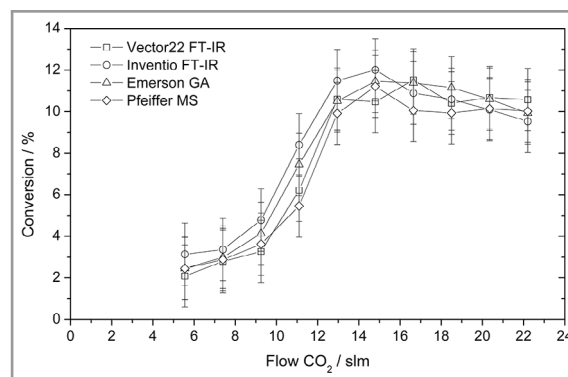


**Figure 3.**  $CO_2$  conversion measured for different  $CO_2$  gas flows at 1.5 kW microwave power with an additional membrane reactor between nozzle and heat exchanger. For comparison four different diagnostics were used. The  $CO_2$  flow was varied from 5.6 to 22.2 slm and the conversion is in the range of 2 % to 12 %.

microwave plasma plant and the two diagnostics with the established process, the same membrane reactor was added to the system. The results of the four diagnostics in two different setups are presented in Fig. 3.

The  $CO_2$  flow was varied at 1.5 kW microwave power from 5.6 to 22.2 slm. The conversion of this setup differs from 2 % up to a maximum of 12 %. At lower  $CO_2$  flows, a lower conversion was measured and an increase until 14.8 slm with a conversion of 12 % was found. This curve can be explained by the membrane reactor. At low gas flow rates, the effluent plasma is not cooled efficiently because the heat exchanger is further away. At higher flows, the cold  $CO_2$  gas quenches the more turbulent effluent plasma. With further increasing flow rates the conversion decreases slightly. All diagnostics show the same trend and the values all lay within the error bars. According to these results the diagnostics are capable of determining the conversion. The two plasma setups with different magnetrons further ensured that the process is robust and repeatable.

The membrane reactor was removed for the remaining experiments as indicated in Fig. 2. The comparison of different  $CO_2$  flows, shown in Fig. 4, demonstrates a decrease of conversion with increasing flow. As a diagnostic tool for this series of measurements the Invenio R FT-IR spectrometer was used. The  $CO_2$  flow was varied from 5.6 up to 74 slm at 1.5 kW. The importance of the quenching position of the heat exchanger can be seen by the comparison of low  $CO_2$  flow rates at 1.5 kW with and without membrane reactor (Figs. 3 and 4). The biggest effect can be seen at 5.6 slm with a conversion of 2 % with the membrane reactor and 18 % without the membrane reactor. At  $CO_2$  flow rates of more than 16.7 slm there was no quenching effect of the heat exchanger. This can be explained through the mixing of cold  $CO_2$  out of the vortex flow and the effluent plasma in the nozzle. At higher flow rates the effluent plasma gets more turbulent behind the nozzle and is not so extended. For higher microwave power small  $CO_2$  flow rates cannot be

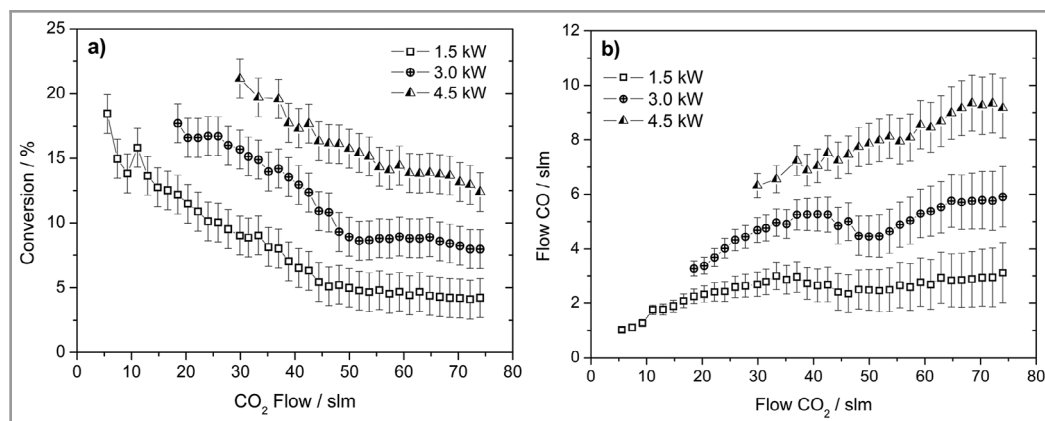


**Figure 4.** CO<sub>2</sub> conversion (a) and produced CO flow (b) at microwave powers between 1.5 and 4.5 kW as a function of CO<sub>2</sub> inlet flow measured with FT-IR. The CO<sub>2</sub> flow was varied from 5.6 to 74 slm with conversions up to 21.1 %. The conversion decreases with higher CO<sub>2</sub> flows and increases with microwave power.

measured, because the vortex flow was not able to stabilize the bigger plasma volume.

The conversion increases with microwave power with the maximum conversion of 21.1 % at 4.5 kW and 29.9 slm. At lower CO<sub>2</sub> flows the conversion declines at a steeper rate than at higher flow rates. In this region, the conversion is almost saturated. At 74 slm the conversion is 4.2 % at 1.5 kW, 8.0 % at 3.0 kW, and 12.4 % at 4.5 kW. In this area the conversion increases approximately linearly with the microwave power. The plotted total amount of produced CO (Eq. (3)) visualizes the rise of product corresponding to the increase of CO<sub>2</sub> flow rates and microwave power. At higher CO<sub>2</sub> flow rates, the total amount of produced CO only slightly increases. The highest amount of produced CO was at a microwave power of 4.5 kW and 72.2 slm CO<sub>2</sub> with a CO product flow of 9 slm. The non-monotonic increase in the CO flow at 1.5 and 3.0 kW is due to the slightly lower conversion between the flows 33.3 and 44.4 slm at 1.5 kW (35.2 and 51.8 slm at 3.0 kW). Due to the calculation of the CO out-

put through the conversion values the error rises with the CO<sub>2</sub> input flow rate. Small differences in conversion have a big impact at higher CO<sub>2</sub> flow rates on the calculated CO output. These results highlight the potential for upscaling according to preferred process parameters of high flow rates and microwave powers.

The resulting EEs (Eq. (5)) of the varied CO<sub>2</sub> flow rates between 5.6 and 74 slm are depicted in Fig. 5a. Increasing the CO<sub>2</sub> flow results in a higher EE. The maximum EE was found at 74 slm with 40.2 %. At small CO<sub>2</sub> flows lower microwave powers lead to greater energy efficiencies. This can be explained by the more effective quenching at lower microwave power. The lowest EE was measured at 5.6 slm CO<sub>2</sub> with 13.2 %. This indicates that high flow rates have a more favored outcome. The same non-monotonic behavior as with the CO flow was observed. At these flows the energy efficiency becomes independent of the microwave power resulting in the flexibility of the process parameter range. Renewable intermittent energies show big fluctuations in

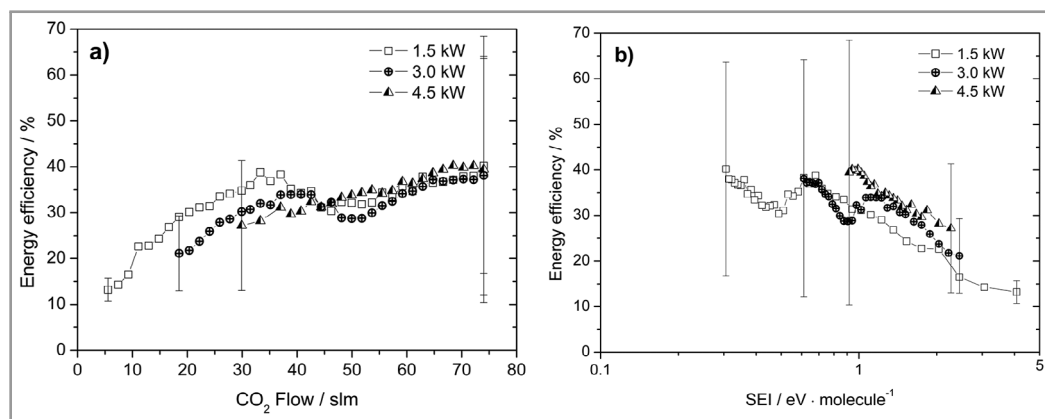


**Figure 5.** Energy efficiencies for microwave power between 1.5 and 4.5 kW versus the CO<sub>2</sub> flow between 7.4 and 74 slm (a) and the logarithmic SEI (b). The energy efficiency increases with higher CO<sub>2</sub> flows and lower SEI. The error bars are only shown for specific values to remain the clarity and show the trend.



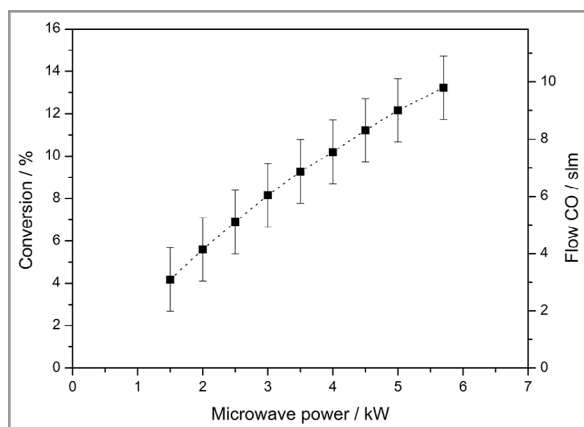


**Figure 6.** CO<sub>2</sub> conversion (left axis) as a function of microwave power at a CO<sub>2</sub> flow of 74 slm measured with the Emerson gas analyzer. The microwave power was varied from 1.5 up to 5.7 kW. Right axis: total amount of produced CO.

generated power and these fluctuations can be used by this microwave plasma process to convert CO<sub>2</sub> without losing efficiency over a big range of power. All three tested microwave powers show a rise in EE with decreasing SEI, as displayed in Fig. 5b. The maximum efficiency of 40.2 % was calculated at an SEI of 0.9 eV molecule<sup>-1</sup>. This value was found at 4.5 kW and nearly the same efficiencies were detected for 3.0 kW at an SEI of 0.6 eV molecule<sup>-1</sup> and for 1.5 kW at 0.3 eV molecule<sup>-1</sup>.

The dependency of microwave power on the conversion at highest flow rate is illustrated in Fig. 6. The microwave power was varied from 1.5 kW up to 5.7 kW at a CO<sub>2</sub> flow of 74 slm. The conversion steadily increases from 4 % at 1.5 kW up to 13.2 % at 5.7 kW. The total amount of produced CO increases with power. At 1.5 kW a product flow of 3.1 slm was achieved. The maximum CO flow of 9.8 slm was produced at 5.7 kW, which is the highest amount of power of the magnetron. In addition, 74 slm is the highest flow rate that can be achieved with the setup presented and the flow meters and two gas inlets used. The plasma process reaches a flexible use of power at high flows without losing efficiency.

The same resonator setup without a nozzle from Wiegers et al. [19] showed a maximum conversion of 8 % and energy efficiency of 25 %. With different nozzles Wiegers et al. increased the CO<sub>2</sub> conversion up to 21 % and the EE up to 35 % [25]. Both setups were tested at microwave powers up to 1.6 kW. In this work, the microwave power was varied up to 5.7 kW. A maximum conversion of 21.1 % and energy efficiency of 40 % was measured. Increasing the CO<sub>2</sub> flow rate results in a decrease of conversion. The same trend was found by Hecimovic et al. [13] at 900 mbar and up to 30 slm. Furthermore, the almost linear scale of conversion with increasing microwave power up to 3.0 kW was identified. Belov et al. demonstrated a conversion of 11.3 % at 4.75 kW and a CO<sub>2</sub> flow rate of 15 slm [33]. This conversion is comparable to the achieved values in this work, but

at a lower CO<sub>2</sub> flow rate. In a case study of van Rooij et al. a process scale of up to around 20 000 t \* year<sup>-1</sup> of CO is assumed so that the process has a relevant size for the industry [34]. In a next step for scaling up the microwave plasma process can be the switch to 915 MHz, which leads to higher microwave powers and flow rates.

A CO<sub>2</sub> plasma at 915 MHz was tested by Hong et al. [35]. A stable plasma process at 50 slm and 16 kW was achieved, without measuring the conversion. Bongers et al. reached conversions up to 23 % and energy efficiencies up to 51 % with a 200 mbar plasma at 915 MHz at 75 slm CO<sub>2</sub> [29]. The used resonator is a similar, upscaled version to the one presented in this work. CO<sub>2</sub> flow rates up to 75 slm and microwave powers of up to 10 kW were investigated. For an industrial process atmospheric pressure is favorable to low-pressure systems because of a higher throughput. Future experiments can be conducted at 915 MHz and atmospheric pressure as an upscaling step. Furthermore, the used setup can be optimized with change in nozzle design, improved gas quenching or higher microwave power and CO<sub>2</sub> flow rates.

## 4 Conclusion

The splitting of CO<sub>2</sub> into CO and O<sub>2</sub> was achieved with an atmospheric pressure microwave plasma torch. The conversion of the setup was compared to the values achieved by Wiegers et al. [19, 25]. For these experiments, a membrane reactor was added between the nozzle and the heat exchanger to only deviate the magnetron. Both systems showed good reproducible conversions at 1.5 kW and CO<sub>2</sub> flow rates up to 22.2 slm. In this comparison four different diagnostics were tested, namely, two different FT-IR spectrometers, a mass spectrometer, and a gas analyzer. These showed equivalent results and were capable of determining the conversion. The setup described in Wiegers et al. [19, 25] is capable of CO<sub>2</sub> gas flow rates up to 25 slm and microwave powers up to 1.6 kW.

In this work, the setup is upscaled with a 6 kW magnetron. This setup is able to use microwave powers up to 5.7 kW and CO<sub>2</sub> gas flow rates up to 74 slm. The conversion experiments were done with and without the membrane reactor to determine the conversion and energy efficiency. At lower CO<sub>2</sub> flow rates, the setup without the membrane reactor achieved higher conversions due to better quenching of the heat exchanger. At flow rates over 16.7 slm the position of the heat exchanger is not changing the conversion. This can be explained with the mixing of cold CO<sub>2</sub> with the effluent plasma in the nozzle. The setup without the membrane reactor showed that conversion increases with microwave power and decreases with CO<sub>2</sub> input flow, due to less energy per molecule. The maximum conversion achieved was 21.1 % at 4.5 kW and 29.9 slm CO<sub>2</sub>. At a CO<sub>2</sub> flow rate of 74 slm, the highest energy efficiency was measured at 40.2 %. This efficiency was independent of the microwave

power and shows the high flexibility of the plasma process.

The process is capable of retaining the efficiency with the fluctuations of intermittent renewable energies. The maximum produced CO flow was 9.8 slm at 74 slm CO<sub>2</sub> and 5.7 kW. Future experiments could focus on further improving the reactor and nozzle design, gas quenching or upscaling to higher microwave powers and CO<sub>2</sub> flow rates. Also, an additional upscaling step could be an option for future experiments, where the frequency is changed to a 915 MHz magnetron with higher microwave power and larger resonator volume, hence leading to higher gas flow rates.

## Acknowledgment

The authors thank the German Federal Ministry of Education and Research (BMBF) for funding the NexPlas project "NEXT GENERATION PLASMA CONVERSION", project no. FKZ:03SF0618A. The authors also thank Heinz Petto for the technical assistance.

Open access funding enabled and organized by Projekt DEAL.

## Symbols used

$F$	[slm]	flow rate
$p$	[kW]	power

## Greek letters

$\Delta H_R$	[kJ mol <sup>-1</sup> ]	reaction enthalpy
$\chi$	[%]	conversion
$\eta$	[%]	energy efficiency

## Abbreviations

EE	energy efficiency
FT-IR	Fourier-transform infrared
GA	gas analyzer
GHG	greenhouse gas
IR	infrared
MW	microwave
SEI	specific energy input
slm	standard liter per minute

## References

- [1] L. J. R. Nunes, *Environments* **2023**, 10 (4), 66. DOI: <https://doi.org/10.3390/environments10040066>
- [2] H. Lee, et al., *IPCC, 2023: Climate Change 2023: Synthesis Report. Contribution of Working Groups I, II and III to the Sixth*

*Assessment Report of the Intergovernmental Panel on Climate Change* (Eds.: H. Lee, J. Romero), IPCC, Geneva, Switzerland, Vol. 2023, Intergovernmental Panel on Climate Change (IPCC) **2023**.

- [3] United Nations, *Paris Agreement*, United Nations Treaty Collection, Paris **2015**.
- [4] R. Detz, et al., *ChemSusChem* **2024**, 17 (15), e202400059. DOI: <https://doi.org/10.1002/cssc.202400059>
- [5] R. J. Detz, B. van der Zwaan, *Energy Policy* **2019**, 133, 110938. DOI: <https://doi.org/10.1016/j.enpol.2019.110938>
- [6] M. Alhassan, et al., *Environ. Sci. Pollut. Res. Int.* **2024**, 31 (30), 42640–42671. DOI: <https://doi.org/10.1007/s11356-024-34021-2>
- [7] J. Booz, D. Höhner, S. Burmester, in *CO<sub>2</sub> and CO as Feedstock, Circular Economy and Sustainability* (Eds: M. Kircher, T. Schwarz), Springer International Publishing, Cham **2023**.
- [8] J. Chi, H. Yu, *Chin. J. Catal.* **2018**, 39 (3), 390–394. DOI: [https://doi.org/10.1016/s1872-2067\(17\)62949-8](https://doi.org/10.1016/s1872-2067(17)62949-8)
- [9] S. A. Grigoriev, et al., *Int. J. Hydrogen Energy* **2020**, 45 (49), 26036–26058. DOI: <https://doi.org/10.1016/j.ijhydene.2020.03.109>
- [10] R. Snoeckx, A. Bogaerts, *Chem. Soc. Rev.* **2017**, 46 (19), 5805–5863. DOI: <https://doi.org/10.1039/C6CS00066E>
- [11] A. Saravanan, et al., *Chem. Eng. Sci.* **2021**, 236, 116515. DOI: <https://doi.org/10.1016/j.ces.2021.116515>
- [12] R. Küngas, *J. Electrochem. Soc.* **2020**, 167 (4), 44508. DOI: <https://doi.org/10.1149/1945-7111/ab7099>
- [13] A. Hecimovic, et al., *J. CO<sub>2</sub> Util.* **2023**, 71, 102473. DOI: <https://doi.org/10.1016/j.jcou.2023.102473>
- [14] M. Leins, et al., *Contrib. Plasma Phys.* **2012**, 52 (7), 615–628. DOI: <https://doi.org/10.1002/ctpp.201210058>
- [15] M. Leins, et al., *Plasma Process. Polym.* **2009**, 6 (S1), S227–S232. DOI: <https://doi.org/10.1002/ppap.200930604>
- [16] M. Leins, et al., *J. Vis. Exp.* **2015**, 98, e52816. DOI: <https://doi.org/10.3791/52816>
- [17] S. Gaiser, *Diagnostik und Modellierung eines Mikrowellen-Plasmabrenners bei Atmosphärendruck*, Dissertation, University of Stuttgart **2017**.
- [18] E. Klemm, et al., *Can. J. Chem. Eng.* **2022**, 100 (10), 2736–2761. DOI: <https://doi.org/10.1002/cjce.24397>
- [19] K. Wiegiers, et al., *Chem. Ing. Tech.* **2022**, 94 (3), 299–308. DOI: <https://doi.org/10.1002/cite.202100149>
- [20] R. Antunes, et al., *ACS Sustainable Chem. Eng.* **2023**, 11 (44), 15984–15993. DOI: <https://doi.org/10.1021/acssuschemeng.3c04862>
- [21] A. Hecimovic, et al., *J. CO<sub>2</sub> Util.* **2024**, 83, 102825. DOI: <https://doi.org/10.1016/j.jcou.2024.102825>
- [22] A. Hecimovic, et al., *J. CO<sub>2</sub> Util.* **2022**, 57, 101870. DOI: <https://doi.org/10.1016/j.jcou.2021.101870>
- [23] C. K. Kiefer, et al., *Chem. Eng. J.* **2024**, 481, 148326. DOI: <https://doi.org/10.1016/j.cej.2023.148326>
- [24] F. A. D'Isa, et al., *Plasma Sources Sci. Technol.* **2020**, 29 (10), 105009. DOI: <https://doi.org/10.1088/1361-6595/abaa84>
- [25] K. Wiegiers, et al., *Enhancing CO<sub>2</sub> Decomposition and Oxygen Removal via Ceramic Hollow Fibers in a Microwave Plasma Torch*, ISPC 25, Kyoto, **2023**. <https://www.ispc-conference.org/ispcproc/ispc25/pdf/2-P-209.pdf> (Accessed on November 25, 2024)
- [26] G. Chen, et al., *Chem. Eng. J.* **2020**, 392, 123699. DOI: <https://doi.org/10.1016/j.cej.2019.123699>
- [27] D. Kiesler, *Untersuchung zur Skalierbarkeit eines Mikrowellen-Plasmabrenners bei Atmosphärendruck*, Diploma Thesis, University of Stuttgart **2008**.
- [28] J. Kopecki, *Entwicklung und spektroskopische Untersuchung eines Mikrowellen-Plasmabrenners für die Schichtabschei-*

- dung aus Pulvern*, Diploma Thesis, University of Stuttgart **2012**.
- [29] W. Bongers, et al., *Plasma Process. Polym.* **2017**, *14* (6), 1600126. DOI: <https://doi.org/10.1002/ppap.201600126>
- [30] N. Taquet, et al., *Int. J. Greenhouse Gas Control* **2013**, *12*, 359–371. DOI: <https://doi.org/10.1016/j.ijggc.2012.10.003>
- [31] H. Haken, *Molekülphysik und Quantenchemie: Einführung in die experimentellen und theoretischen Grundlagen*, Springer-Verlag, Berlin **2006**.
- [32] H. Vu, M. R. Atwood, B. Vodar, *J. Chem. Phys.* **1963**, *38* (11), 2671–2677. DOI: <https://doi.org/10.1063/1.1733571>
- [33] I. Belov, et al., *J. CO2 Util.* **2018**, *24*, 386–397. DOI: <https://doi.org/10.1016/j.jcou.2017.12.009>
- [34] G. J. van Rooij, et al., *Plasma Phys. Control. Fusion* **2018**, *60* (1), 14019. DOI: <https://doi.org/10.1088/1361-6587/aa8f7d>
- [35] Y. C. Hong, et al., *IEEE Trans. Plasma Sci.* **2011**, *39* (10), 1958–1962. DOI: <https://doi.org/10.1109/TPS.2011.2162969>